



# Friction in Rolling a Cylinder on or Under a Viscoelastic Substrate with Adhesion

R. Nazari<sup>1</sup> · A. Papangelo<sup>1</sup> · M. Ciavarella<sup>1</sup>

Received: 14 February 2024 / Accepted: 2 March 2024  
© The Author(s) 2024

## Abstract

In classical experiments, it has been found that a rigid cylinder can roll both on and *under* an inclined rubber plane with a friction force that depends on a power law of velocity, independent of the sign of the normal force. Further, contact area increases significantly with velocity with a related power law. We try to model qualitatively these experiments with a numerical boundary element solution with a standard linear solid and we find for sufficiently large Maugis–Tabor parameter  $\lambda$  qualitative agreement with experiments. However, friction force increases linearly with velocity at low velocities (like in the case with no adhesive hysteresis) and then decays at large speeds. Quantitative agreement with the Persson–Brener theory of crack propagation is found for the two power law regimes, but when Maugis–Tabor parameter  $\lambda$  is small, the cut-off stress in Persson–Brener theory depends on all the other dimensionless parameters of the problem.

**Keywords** Friction · Adhesion · Viscoelasticity · Rolling · Soft materials · Rubber · Elastomers

## 1 Introduction

In a series of experiments using a long rigid cylinder rolling both upon and *under* inclined viscoelastic rubber substrates, Barquins [1] found that a friction force developed that depends on velocity (in his experiments, as a power law) and his main findings were that (i) the friction force was approximately equal for negative or positive normal force and that (ii) it followed a power law of velocity very similar to what had been found in peeling experiments. This suggested the rolling resistance friction force was due to the presence of strong adhesion leading to a peeling force at the trailing edge of the contact area where the contact edge behaves like an opening crack, while the leading edge is a closing crack since the work restituted is much smaller than that at the trailing edge. Barquins conducted experiments where the rolling velocity was measured as a function of the angle  $\beta$  of inclination of the substrate (see Fig. 1) and consequently (neglecting dissipation in the bulk of the material which is dominant instead at very large normal loads),

the energy release rate difference is directly related to the measured force

$$G(v) = G_{trailing} - G_{leading} = f \sin \theta = f_T, \quad (1)$$

where  $f = mg$  is the vertical force per unit length (see Fig. 1) and  $f_T$  is the tangential component. Notice that the normal load is instead  $w = f \cos \theta$ . Here,  $G_{trailing}$  is the crack propagation energy per unit surface area when the crack moves at the speed  $v$  and  $G_{leading}$  is the energy restituted when the crack is closing.

Barquins [1] in particular found  $G = kv^n$  where the coefficient  $n \simeq 0.55$  was close to the 0.6 found in previous peeling and detachment from flat or spherical punches experiments of the same transparent rubber-like material (polyurethane) in contact with glass [2], and indeed, the entire curve for  $G$  seemed independent of geometrical features.

Later on, Charmet and Barquins [3] have additionally found other interesting aspects of this rolling problem, namely that

(iii) rolling was possible under negative loads with an increase of 50 times of the friction force measured between the low and the fast velocities in the experiments. Aligning the negative and positive loads, 4 orders of magnitudes were varied in speed and about 2 orders of magnitude in force, with experiments never showing deviations from this power law;

✉ M. Ciavarella  
Mciava@poliba.it

<sup>1</sup> Department of Mechanics, Mathematics and Management, Politecnico di Bari, Via Orabona 4, 70125 Bari, Italy

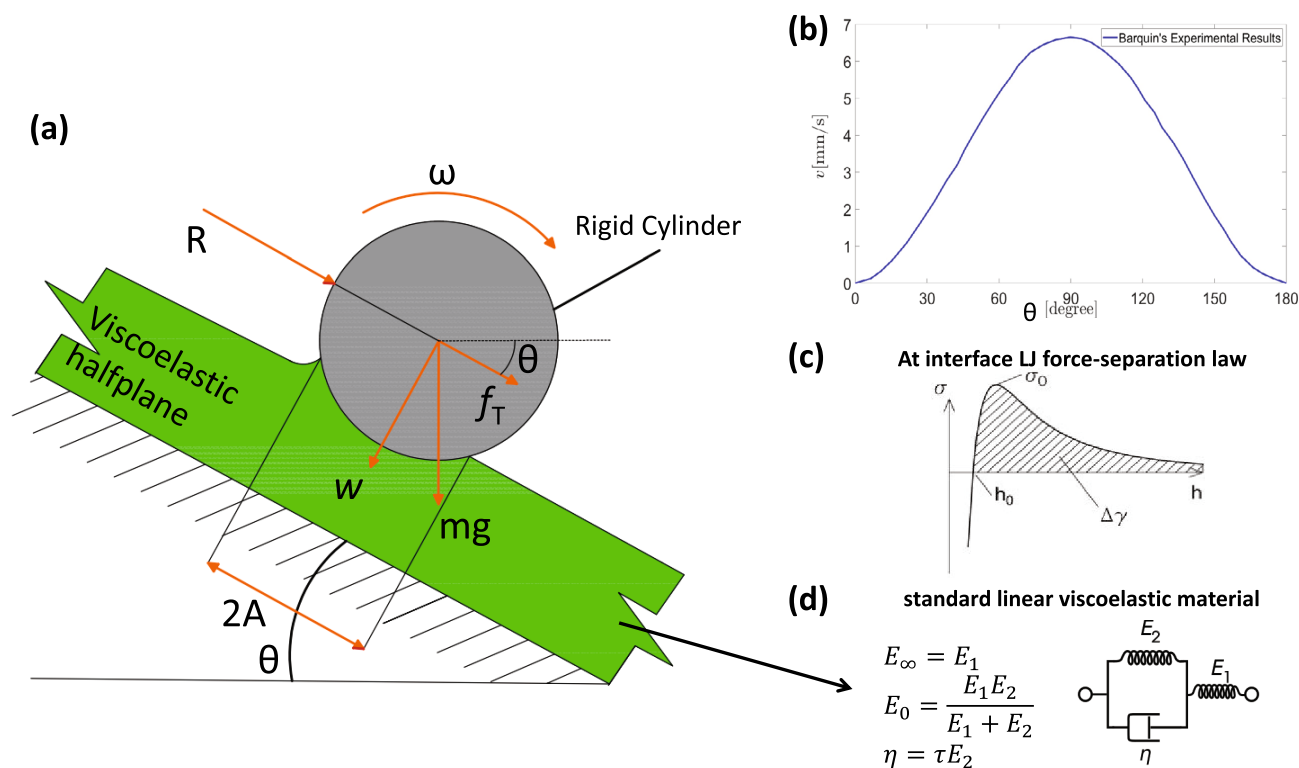


**Fig. 1** Barquins’ experiments: **a** the rigid cylinder rolling above or under an inclined viscoelastic rubber substrate; **b** a sketch of the experimental velocities obtained as a function of the inclination

(iii) that the contact area half-width size was scaling as  $a = k_2 v^{n/3}$  and a tentative explanation was given.

Unfortunately, Barquins did not give a full characterization of the viscoelastic modulus of his polyurethane rubbers, so we can only make qualitative assessment of his experiments, and indeed for simplicity we shall consider a standard linear solid for most of our work, although we shall make also some discussion about a possible power law solid model.

The evidence of these main findings (i–ii–iii–iiii) has never been compared with a theoretical/numerical prediction, in the best of the authors’ knowledge, and for this purpose we shall here study the adhesive contact problem of a cylinder rolling on a viscoelastic half-plane using a Lennard–Jones force separation law and a boundary element formulation. We find friction due both to viscoelastic losses in the bulk (in the limit case of absence of adhesion, a full theory exists [4]) as well as the adhesive contribution due to the difference between the enhanced adhesion at the opening crack (trailing edge of contact) and the reduced adhesion at the closing crack (leading edge of contact). The different behaviors of closing or opening viscoelastic cracks are well known for semi-infinite cracks [5, 6] for which the size of the cohesive zone is much smaller than any other length scale in

angle; **c** the Lennard–Jones adhesion force separation law adopted in this numerical work; and **d** the standard solid material viscoelastic model

the problem, so one of these theories (the Persson–Brener one [6]) will be used to attempt to interpret our results for the present problem.

Our analysis will not make specific assumption about the range of adhesive forces, for which adhesive problems show a transition between long-range (small  $\lambda$ ) and short-range (large  $\lambda$ ) type of adhesion, depending to the Tabor–Maugis parameter [7, 8]

$$\lambda = \sigma_0 \left( \frac{R}{\Delta\gamma E_0^*} \right)^{1/3}, \tag{2}$$

where we made reference to the plane strain *relaxed* elastic modulus of the material,  $E_0^* = \frac{E_0}{1-\nu^2}$  where  $\nu$  is the Poisson’s ratio and  $\sigma_0$  is cohesive (or theoretical strength) stress,  $\Delta\gamma$  surface energy (energy to break the adhesive bonds per unit surface area),  $R$  is the cylinder radius, while  $E_0$  is the standard Young’s modulus at low frequencies. In the classical elastic adhesive problem of spherical geometry, large spheres with soft material show large  $\lambda$  ( $\lambda > 5$  is generally sufficient to consider “short-range” adhesion) we can apply Linear Elastic Fracture Mechanics of the Griffith energy balance approach (JKR limit). On the contrary, for

small spheres and stiff material, small  $\lambda$  makes an energetic approach invalid and there is a tendency toward the limit of rigid material adhesion. In the present case of rolling cylinder, we expect that long-range adhesion will make friction mostly dependent on bulk dissipation, while short-range adhesion will increase adhesive effects and make the adhesive hysteretic contribution dominant. The adhesive contact in the elastic case for the cylinder has been studied, for example, by Johnson and Greenwood [9] and by Wu [10], whose notation and also the main algorithm we shall follow, extending it to viscoelastic material in steady-state sliding by changing the Green function.

For viscoelastic materials, the JKR limit cannot be defined and a cohesive model is always needed, because at the contact edge (which corresponds to a crack tip), the strain rate in a propagating crack is always infinite and therefore without a cohesive model we would not see a dependence of crack/contact edge velocity on the applied load, contrary to experimental evidence.

The influence of the Tabor–Maugis parameter in viscoelastic contact problems has been shown to be large, because typically only large  $\lambda$  lead to strong amplification of the pull-off load and of viscoelastic effects [11, 12], and pull-off loads, for example, for a sphere, can be increased due to loading rate effect of a factor up to the theoretical limit of  $1/k = E_\infty/E_0$  (which is often of the order of  $10^3$  for rubbers), where  $E_\infty$  is the high-frequency (instantaneous) modulus of the material. However, in the rolling problem, the effect of Tabor parameter has not been considered so far, particularly to check the range of validity of the Persson-Brener theory [6]. We therefore describe in detail the model next, we give comprehensive results and compare with the experimental results of Barquins.

## 2 The Model

We consider a rigid cylinder of radius  $R$  in steady rolling with its center moving with peripheral velocity  $v$  over an adhesive viscoelastic half-plane and assume friction is not due to shear tractions, but to inclined pressures in the contact area as we detail later. We extend the elastic adhesive solution by Wu [10] for both viscoelasticity and the presence of steady-state sliding.

We introduce a Lennard–Jones (LJ) force separation law, so that the stress between the two interacting surfaces  $p(h)$  is

$$p(h) = -\frac{8\Delta\gamma}{3\epsilon} \left[ \left(\frac{\epsilon}{h}\right)^3 - \left(\frac{\epsilon}{h}\right)^9 \right], \tag{3}$$

where  $h$  is the local gap between the two surfaces,  $\epsilon$  is the equilibrium distance,  $\Delta\gamma = \zeta\sigma_0\epsilon$  is the surface energy,  $p < 0$  when tensile and  $\zeta = 9\sqrt{3}/16 \approx 0.9743$ .

The gap function is

$$h(x) = -\delta + \epsilon + \frac{x^2}{2R} + u_z(x, v), \tag{4}$$

where  $\delta$  is the indentation ( $\delta > 0$  when rigid cylinder approaches the substrate) and the half-plane deflections  $u_z(x, v)$  depend not only on the in-plane coordinate but also on the velocity  $v$ . We introduce the adhesive length parameter

$$\beta = \left( \frac{R^2\Delta\gamma}{E_0^*} \right)^{1/3}. \tag{5}$$

and the dimensionless parameters

$$\begin{aligned} \Delta &= \frac{\delta R}{\beta^2}; & H &= \left( \frac{h}{\epsilon} - 1 \right) \frac{R\epsilon}{\beta^2}; & X &= \frac{x}{\beta}; \\ P &= \frac{p}{\sigma_0}; & U &= \frac{u_z R}{\beta^2}; & W &= \frac{w}{(E_0^* R \Delta \gamma^2)^{1/3}}. \end{aligned} \tag{6}$$

Hence, we write a dimensionless gap function and LJ force separation law as

$$H = -\Delta + \frac{X^2}{2} + U(X, V), \tag{7}$$

$$P(h) = -\frac{3\sqrt{3}}{2} \left[ \frac{1}{(H+1)^3} - \frac{1}{(H+1)^9} \right]. \tag{8}$$

The solution of the contact problem is found with the described boundary element method similarly to the implementation in Refs. [13, 14]. In particular, the domain of length  $L$  is discretized in  $M$  uniformly spaced elements of size  $2b = L/M$ , corresponding to  $N = M$  interfacial nodes. Nodal deflections are obtained using the Green function for a constant pressure element of dimension  $2b$  steadily moving at velocity  $v$  on a half-plane constituted by a linear standard viscoelastic material with a single relaxation time, which, in dimensionless form, reads [15]

$$\begin{aligned} U(X, V) = & -\frac{2\lambda}{\pi} P \left\{ \frac{\pi}{2} D - \frac{k}{2} \left[ (X+B) \ln \left( \frac{X+B}{B} \right)^2 \right. \right. \\ & \left. \left. - (X-B) \ln \left( \frac{X-B}{B} \right)^2 \right] \right. \\ & + \frac{(1-k)}{2} \left[ 2V \exp \left( \frac{X+B}{V} \right) \text{Ei} \left( -\frac{X+B}{V} \right) \right. \\ & \left. - (X+V+B) \ln \left( \frac{X+B}{B} \right)^2 \right] \\ & \left. - \frac{(1-k)}{2} \left[ 2V \exp \left( \frac{X-B}{V} \right) \text{Ei} \left( -\frac{X-B}{V} \right) \right. \right. \\ & \left. \left. - (X+V-B) \ln \left( \frac{X-B}{B} \right)^2 \right] \right\} \end{aligned} \tag{9}$$

being  $B = b/\beta$ ,  $V = v\tau/\beta$ ,  $k = E_0/E_\infty$ , and  $Ei(\cdot)$  the exponential integral function and  $D = d/\beta$  an arbitrary chosen constant to set the datum point of the displacement field: the load versus displacement curves depend on the choice of the datum point, but the relation between the load  $W$  and the gap  $H(X = 0)$ , does not. We shall assume  $D = 0$ . Using superposition and Eq. (9), we obtain the influence matrix  $[G]_{N \times N}$  and deflections at every node due to an arbitrary pressure distributions are

$$\{U\}_{N \times 1} = \left(\frac{2\lambda}{\pi}\right)[G]_{N \times N}\{P\}_{N \times 1}. \tag{10}$$

The problem is highly nonlinear due to the dependence of  $P$  on the  $H$  via the LJ law. Hence, the contact problem [(Eqs. (7,10,8))] is solved numerically using an iterative Newton–Raphson scheme implemented in the software MATLAB.

### 2.1 Friction Force

The case of an adhesiveless cylinder rolling over a viscoelastic half-plane has been solved by Persson [4], giving

$$\mu_{noadh} = \frac{a_0}{R}g\left(\frac{v\tau}{a_0}, k\right) = \sqrt{\frac{4W}{\pi}}\left(\frac{\sigma_0}{\lambda E_0^*}\right)g\left(\frac{v\tau}{a_0}, k\right), \tag{11}$$

where  $g\left(\frac{v\tau}{a_0}, k\right)$  is a function which is detailed in Persson [4] and has a bell shape, rising initially linearly with velocity and then reaching a maximum of about  $g\left(\frac{v\tau}{a_0}, k\right) = 0.5$  for the common case of  $k < 0.1$ , and  $a_0$  is the contact half-width at zero speed in the Hertz solution (no adhesion). Friction coefficient depends on normal load in general, but near zero normal load, it is better to express the frictional force since this is nearly independent on normal load, while friction coefficient has a singularity near zero load.

In our adhesive case, we solve the problem to obtain the load for various approaches  $\Delta$  and for any given solution, we obtain the pressure and the displacements fields in the entire domain. The friction force is then given by the integral (assuming, for example, the case of  $\theta < \pi/2$  when rolling is from left to right and trailing edge is on the left side)

$$f_T = - \int p(x) \frac{du}{dx} dx \tag{12}$$

and hence in dimensionless terms

$$F_T = \frac{f_T}{(E_R^* R \Delta \gamma^2)^{1/3}} = -\sqrt{\lambda^3 \alpha \frac{\epsilon}{R}} \int P(X) \frac{dU}{dX} dX. \tag{13}$$

Interestingly, for the same reason that in the adhesiveless case (11)  $\mu_{noadh} \frac{R}{a_0}$  depends on the minimal number of dimen-

sionless parameters (two in that case), also in the adhesive case

$$F_T^* = F_T \frac{R}{a_0} = -\frac{\sqrt{\pi}}{2} \frac{\lambda}{W^{1/2}} \int P(X) \frac{dU}{dX} dX \tag{14}$$

has the advantage that depends only on the four dimensionless parameters of the problem:

$$F_T^* = F_T^*(V_0, \lambda, W, k), \tag{15}$$

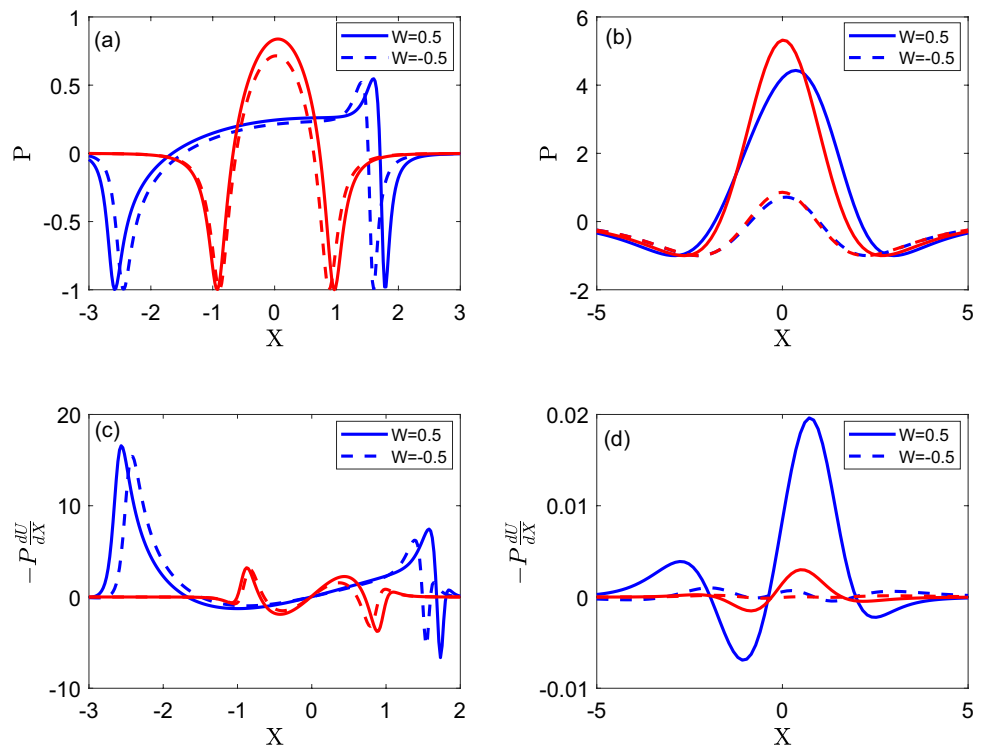
where we introduced the dimensionless speed

$$V_0 = \frac{v\tau}{a_0} = \frac{1}{2} \sqrt{\frac{\pi}{W}} \frac{v\tau}{\beta}, \tag{16}$$

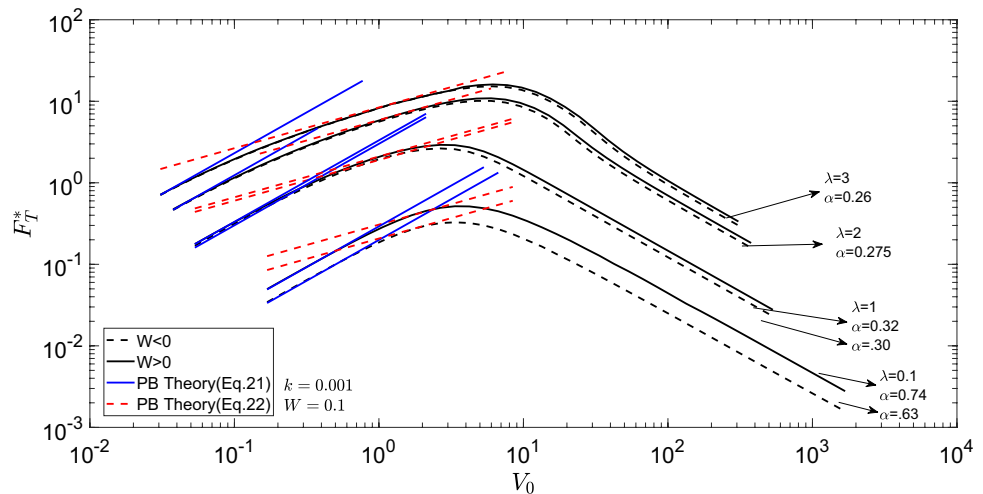
where  $a_0$  is still the Hertzian (adhesiveless) contact half-width of the contact. Apart from  $V_0$ , the dimensionless friction force  $F_T^*$  depends on the Tabor–Maugis parameter  $\lambda$ , the dimensionless load  $W$ , and the ratio between relaxed and instantaneous modulus of the material,  $k = E_0/E_\infty$ . However, we shall see that at low velocities, at least in the range of parameters where the theory of semi-infinite cracks of Persson–Brenner works in full form, the dependence of the friction force is even simpler.

Figure 2 shows the effect of Maugis–Tabor parameter on the pressure distribution (a,b) and the quantity  $-P(X) \frac{dU}{dX}$  which has to be integrated in (14) to obtain the dimensionless friction force  $F_T^*$ . As it can be clearly seen, the pressure exhibits with much sharper tensile peaks for the large  $\lambda$  case (short-range adhesion) (Fig. 2a) than for low  $\lambda$  (long-range adhesion) (Fig. 2b). Moreover, the pressure distribution is nearly independent on the sign of the normal load in the former case (Fig. 2a) than in the latter (Fig. 2b) and has a compressive peak near the leading edge typical of viscoelastic rolling. Moreover, the pressure is nearly symmetrical for large speeds, which is due to the fact that at large speeds the material behaves nearly elastically (with high-frequency modulus) and therefore, the energy release rate at the two ends of the contact is nearly equal, so that we expect friction force to be negligible at large speeds. The plots of the quantity  $-P(X) \frac{dU}{dX}$  permit to see where friction comes from. It is clear from Fig. 2c that large friction occurs for intermediate speeds (here,  $V_0 = 1$ ) due to the large contributions from the trailing edge, while at the leading edge the quantity is smaller and has positive and negative contributions. For large speeds (here,  $V_0 = 100$ ), it is confirmed that friction will be small because it results from integrating a quantity which oscillates and is small anyway. Moving to consider the small Maugis–Tabor parameter case (Fig. 2b,d), friction has bigger contribution from the middle of the contact area (bulk dissipation) than from the edges, since adhesion is small

**Fig. 2** The pressure distribution (a, b) and the quantity  $-P(X)\frac{dU}{dX}$  which has to be integrated in (14) to obtain the dimensionless friction force  $F_T^*$ . Here, trailing edge on the right, and we use standard material with  $k = E_0/E_\infty = 0.001$  and Maugis–Tabor parameter is high  $\lambda = 3$  on (a, c) and low  $\lambda = 0.1$  on (b, d). Notice that dashed lines indicate negative normal load and solid lines positive normal loads. Finally, blue line is  $V_0 = 1$  and red line is  $V_0 = 100$  (Color figure online)



**Fig. 3** The dimensionless friction force  $F_T^*$  as a function of dimensionless velocity  $V_0 = \frac{v\tau}{a_0}$  with standard material with  $k = E_0/E_\infty = 0.001$  showing two power law regimes for low velocities ( $V_0^1$  with blue solid line,  $V_0^{0.5}$  with red-dashed line). Here, the normal load is  $|W| = 0.1$  ( $W > 0$ —black solid line,  $W < 0$  black-dashed line). Four values of Maugis–Tabor parameter are shown,  $\lambda = 0.1, 1, 2, 3$  (Color figure online)



for this case. Moreover, a change in the sign of the normal force changes friction significantly.

### 3 Friction Force Results and Results Using Persson–Brener’s Theory

Figure 3 plots the dimensionless friction force  $F_T^*$  as a function of dimensionless velocity  $V_0 = \frac{v\tau}{a_0}$  with a standard material with a typical value of  $k = E_0/E_\infty = 0.001$ , with four values of Maugis–Tabor parameter  $\lambda = 0.1, 1, 2, 3$  covering

the transition from the long-range to the short-range adhesion regimes. The curve shows a non-monotonic trend, increasing at low speeds, and decreasing at large speeds, with a maximum not too far from  $V_0 = 1$ . In particular, there seem to be two power law regimes for low velocities ( $F_T^* \propto V_0^1$  with blue solid line) and intermediate velocities ( $F_T^* \propto V_0^{0.5}$  with red-dashed line). In the range of low velocities, also the adhesiveless theory of friction due to bulk viscoelastic losses alone by Persson [4] predicts a linearity with the velocity.

In Fig. 3, the normal load is  $|W| = 0.1$  ( $W > 0$ —black solid line,  $W < 0$  black-dashed line) and the curves show



that our numerical results do justify the experimental finding that the friction force is approximately the same for rolling above or under the inclined plane (for same inclination  $\theta$ ), but only if Maugis–Tabor parameter is sufficiently high, namely greater than about  $\lambda = 2$ . For lower  $\lambda$  (which is unlikely to be the case in Barquins’ experiments), there is instead a certain discrepancy/dependence on normal load sign. Notice that the dimensionless friction force increases with the Maugis–Tabor parameter.

These findings motivate us to search for some general pattern elaborating from the Persson–Brener theory, as we do in the next paragraph.

### 3.1 Estimate from the Persson–Brener Model

Considering Eq. 1, classical theories can be used to estimate  $G_{trailing}, G_{leading}$ . As long as the cohesive zone is not too large, and therefore up to velocities close to the maximum in the friction force, and considering that it has been shown [6] that to a very good approximation,  $G_{leading}(v) \simeq 1/G_{trailing}(v)$ , we can use the Persson–Brener theory which gives  $G_{trailing}(v)$  as proportional to the cut-off region size  $c(v)$  within which the stresses are constant and given by cut-off stress  $\sigma_c$ . Notice that this cut-off stress does not correspond to the cohesive strength in our Lennard–Jones model, and indeed even in the case of cracks, cohesive models do depend on the shape of the cohesive law mostly as a shift in the velocity scale [16, 17] and therefore, we need to investigate this point fully numerically also with respect to the Persson–Brener’s model. The PB model states that  $\frac{G_{trailing}(v)}{\Delta\gamma} = \frac{c(v)}{c_0}$  and for a standard material, it leads to the following implicit equation for  $\frac{c(v)}{c_0}$ ,

$$\frac{c(v)}{c_0} = \left[ 1 - \left( 1 - \frac{E_0}{E_\infty} \right) \left( \sqrt{1 + \left( \frac{c_0}{c(v)} \frac{v}{v_0} \right)^{-2}} - \left( \frac{c_0}{c(v)} \frac{v}{v_0} \right)^{-1} \right) \right]^{-1} \quad (17)$$

The difference between trailing and leading energy leads to the results in Fig. 4, which can be approximated as

$$\frac{f_T(v)}{\Delta\gamma} \simeq \frac{G_{trailing}(v) - 1/G_{trailing}(v)}{\Delta\gamma} \simeq \begin{cases} v/v_0, & v < v_0 \\ (v/v_0)^{1/2}, & v > v_0 \end{cases} \quad (18)$$

where  $v_0 = c_0/(2\pi\tau)$  and the fracture process zone at zero speed is defined as

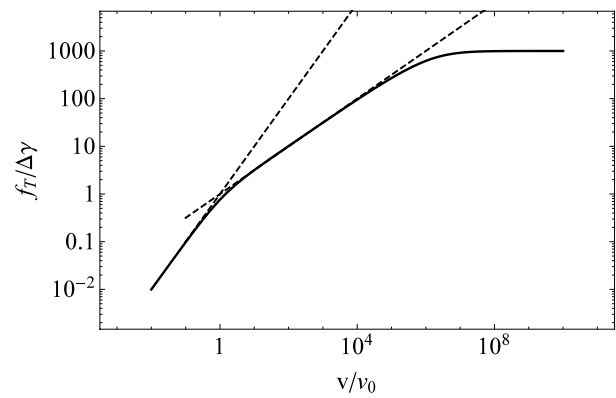


**Fig. 4** The friction force estimated from the Persson–Brener theory for a semi-infinite crack, with standard material with  $k = E_0/E_\infty = 0.001$ , showing two power law regimes at very low and intermediate velocities, which explain approximately the results of Fig. 3

$$c_0 = \frac{E_0 \Delta\gamma}{2\pi\sigma_c^2} \quad (19)$$

which is a very small quantity (actually, being usually even less than nanometers this poses some questions on the validity of the theory since it is smaller than any real feature in the material, see Hui et al. [18]). From the PB theory, therefore, one could define a new dimensionless friction force in terms of the fracture energy,  $F_{T,PB} = \frac{f_T(v)}{\Delta\gamma} = F_{T,PB}(V_{PB})$  and it would then depend only on a *single dimensionless parameter*, the dimensionless velocity  $V_{PB} = v/v_0$ . Therefore, we have interest to investigate where it is possible to simply adopt PB’s theory in view of the simplicity of the results.

To this scope, we need to investigate the relationship between  $\sigma_c$  and the cohesive stress of our cohesive model  $\sigma_0$ , so let us write it in terms of an unknown prefactor

$$\sigma_c = \alpha\sigma_0. \quad (20)$$

The simple result in Fig. 4 are highly reminiscent of our numerical results in Fig. 3. Indeed, using our dimensionless notation (6,16), the PB prediction in the very low velocities range can be rewritten as (using the Hertz equation

$$a_0 = \sqrt{\frac{4wR}{\pi E_0^*}} = \frac{2}{\sqrt{\pi}} \beta \sqrt{W} \\ F_{T1}^* = (2\pi)^2 \alpha^2 \lambda^2 V_0 \quad (21)$$

where notice that since  $V_0 \propto \sqrt{\frac{1}{W}}$  [see Eq.(16)], the dimensionless force really depends on normal load, but it is evident from the Persson–Brener theory that the dimensional force does not.

In the intermediate range of velocities instead

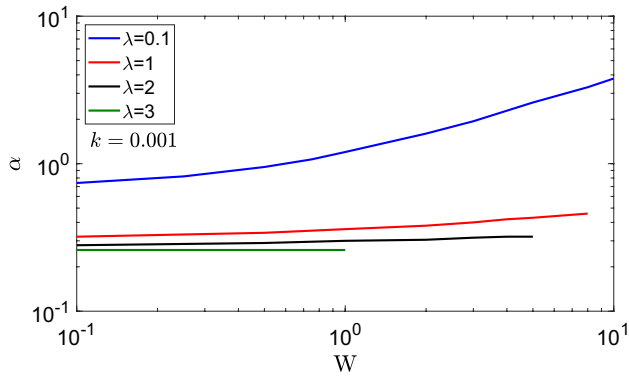


**Fig. 5** The prefactor  $\alpha$  linking the peak of cohesive force in our Lennard–Jones cohesive model with the Persson–Brener cut-off stress as a function of dimensionless normal load  $W$ , with  $k = E_0/E_\infty = 0.001$  and  $\lambda = 0.1, 1, 3$  showing different  $\alpha$  are needed only for low  $\lambda$  (Color figure online)

$$F_{T2}^* = \pi \sqrt{2\pi} \frac{\alpha \lambda}{W^{1/4}} \left(\frac{1}{\pi}\right)^{1/4} V_0^{1/2}. \tag{22}$$

The predictions of Eqs. (21,22) are shown in Fig. 3, where it is found that with  $k = E_0/E_\infty = 0.001$  and  $\lambda = 0.1, 1, 3$ , the PB equations work well at low or intermediate velocities, but different  $\alpha$  are needed depending on  $\lambda$  changing of a factor about 3, and the linear regime is particularly extensive for low  $\lambda$ , while it is more reduced for large  $\lambda$ . Since large  $\lambda$  is more likely to correspond to experiments, this may justify why the linear regime was not really observed. On the other hand, probably the large velocities were also not experimentally available, and hence, only the intermediate power law was observed.<sup>1</sup>

Figure 5 additionally shows that the prefactor  $\alpha$  does *not* depend on the normal load for large Maugis–Tabor parameter (here, we consider the realistic case of  $k = E_0/E_\infty = 0.001$ ).

Also, Fig. 6 shows that  $\alpha$  is nearly independent on normal load for large Maugis–Tabor parameter and decays with  $\lambda$  but remains about constant for  $\lambda > 2$ .

Finally, Fig. 7 shows that  $\alpha$  is nearly independent on  $k = E_0/E_\infty$  for  $k < 0.1$ , which is a quite reasonable range as many materials show rather  $k < 10^{-3}$ , showing that in conclusion the Persson–Brener estimate is a very good fit of our numerical results *for a wide range of conditions*, namely low to intermediate normal loads, realistic instantaneous to

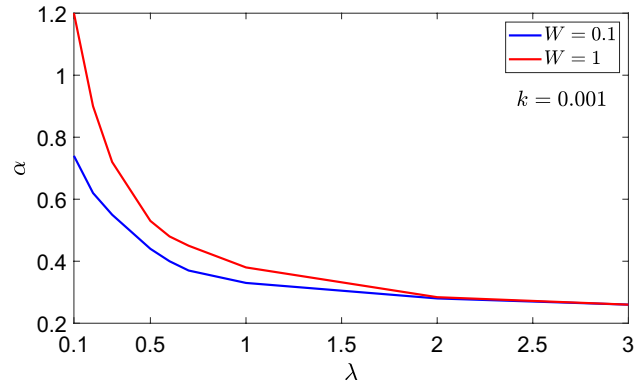


**Fig. 6** The prefactor  $\alpha$  linking the peak of cohesive force in our Lennard–Jones cohesive model with the Persson–Brener cut-off stress as a function of Maugis–Tabor parameter  $\lambda$  showing convergence for large  $\lambda$  (Color figure online)

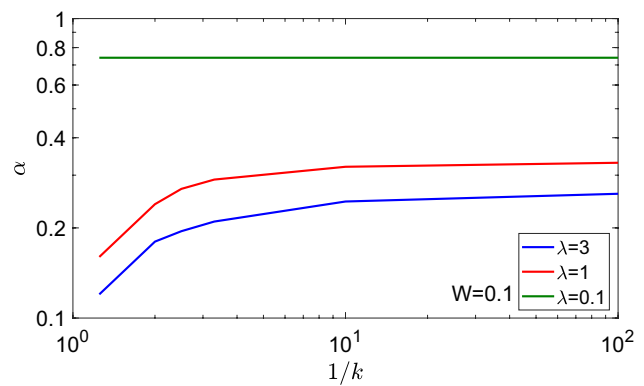


**Fig. 7** The prefactor  $\alpha$  as a function of  $1/k$  for  $W = 0.1$  and various  $\lambda$  (Color figure online)

relaxed modulus of material, and realistically high Maugis–Tabor parameters.

### 4 Discussion: More Complex Material Models

Our model found some qualitative agreement with the results of [1–3], particularly as the fracture energy seems to increase with a power  $V^{0.5}$  which is close to the  $V^{0.55}$  found in rolling experimentally. However, this may be partly a coincidence, and it is unlikely that the rubber used by Barquins was really close to a single relaxation time material. Indeed, when we check the prediction of the contact area, we find greater discrepancies. Figure 8 plots the dimensionless contact area  $2A$  as a function of  $V_0$  for  $k = 0.001$  and normal load set to pull-off value. Barquins had found a power law  $A \sim V_0^{n/3} = V_0^{0.55/3}$  but here we find a much weaker

<sup>1</sup> As in the experiments we are modeling there was no evidence of the decaying branch of the friction force, we did not put effort into modeling this, which may require additional effort of theories, see Persson [19, 20] which is based on limiting the dissipation zone of the Persson–Brener theory based on the size of the contact area or Carbone et al. [21] which surprisingly seems not to contain reference to the cohesive strength of the adhesion law.

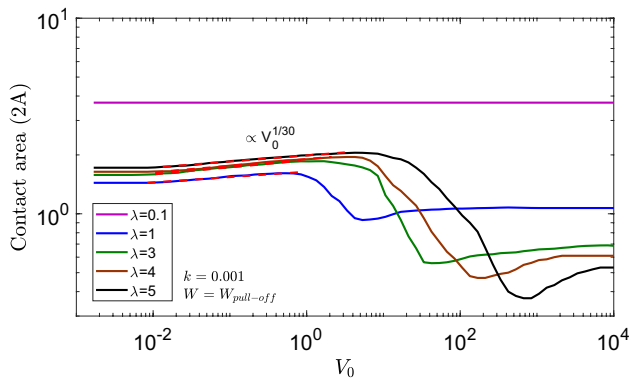


**Fig. 8** The dimensionless contact area  $2A$  as a function of  $V_0$  for  $k = 0.001$  and normal load set to pull-off value (Color figure online)

dependence  $A \sim V_0^{1/30}$  in the range where we do observe the power law at intermediate velocities. Notice that the choice of setting the normal load equal to the pull-off load should not affect the results in the range of large  $\lambda$  since we are in a regime where the normal load is low and the contact area size is mainly governed by adhesive forces, which increase for low to intermediate velocities.

In view of these discrepancies and limitation in our model, it would not be too difficult to extend the study to a material with various relaxation times,<sup>2</sup> but since unfortunately, we do not know precisely the full characterization of the transparent polyurethane rubber Barquins was using in his experiments, this would be not very useful. We can provide a discussion considering a power law material in the following paragraph.

### 4.1 Power Law Materials

To investigate the role of material constants in the case of a more realistic rubber, Persson–Brener suggest power law materials with spectral density function

$$S(\tau) = S_0 \tau^{-s} \tag{23}$$

in  $\tau_1 < \tau < \tau_2$  and zero otherwise, which leads to a complex viscoelastic modulus  $E(\omega)$  which PB say increases as  $\omega^{1-s}$  ( $0 < s < 1$ ). More precisely,  $S(s)$  is defined from the relationship

$$\begin{aligned} \frac{1}{E(\omega)} &= \frac{1}{E_\infty} + \int_0^\infty d\tau \frac{S(\tau)}{1 - i\omega\tau} \\ &= \frac{1}{E_\infty} + S_0 \int_{\tau_1}^{\tau_2} d\tau \frac{\tau^{-s}}{1 - i\omega\tau} \end{aligned} \tag{24}$$

$$\begin{aligned} &= \frac{1}{E_\infty} + S_0 \frac{(-i)^{1-s}}{\omega^{1-s}} \\ &\quad \left( B\left(-\frac{i}{\omega\tau_2}, s, 0\right) - B\left(-\frac{i}{\omega\tau_1}, s, 0\right) \right) \end{aligned} \tag{25}$$

where  $B()$  is the Euler beta function.

This results in PB theory leads to a fracture energy

$$\begin{aligned} \frac{G(v)}{\Delta\gamma} &= \frac{c(v)}{c_0} = \left[ 1 - E_0 \int_0^\infty d\tau S(\tau) \right. \\ &\quad \left. \left( \sqrt{1 + b(\tau)^{-2}} - b(\tau)^{-1} \right) \right]^{-1}, \end{aligned} \tag{26}$$

where  $b(\tau) = 2\pi v\tau/c$ .

PB suggest that most rubbers would have a large spectrum band, i.e., large ratio between  $\tau_1$  and  $\tau_2$  and  $s = 0.6$  approximately so that their full theory leads approximately to  $\frac{G}{\Delta\gamma} \sim v^n$  with

$$n = \frac{1-s}{2-s} \tag{27}$$

meaning  $n = \frac{1-0.6}{2-0.6} = 0.29$ . This would not improve our fit of the Barquins–Maugis polyurethane, since their experimental results with tape peeling, and detachment of flat or spherical punches all suggested  $n = 0.6$  and also the rolling experiment shows  $n = 0.55$ . It would seem therefore

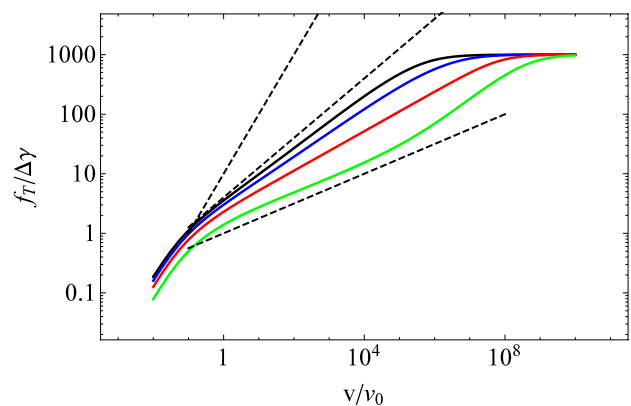


**Fig. 9** The friction force estimated from the Persson–Brener theory for a power law material having  $\tau_1 = 10^{-6}s$  and  $\tau_2 = 1s$  (entanglement time),  $E_0/E_\infty = 0.001$ , and showing  $s = 0, 0.25, 0.5, 0.75$  (solid black, blue, red, and green lines), where the three dashed black lines are indicating the equations  $f_T/\Delta\gamma = 10v/v_0, 4(v/v_0)^{1/2}, (v/v_0)^{1/4}$ , respectively (Color figure online)

<sup>2</sup> An interesting comparison between the theory and experiments of rolling friction for a very detailed viscoelastic material model without adhesive effects is done in [22]



that we would need to use  $s = 0$  to reproduce the power law of [1–3] with a power law material. However, this would really not change results much with respect to the standard material used so far in our paper. Indeed we have estimated for  $v_0 = a_0/(2\pi\tau_2)$  the results of Fig. 9, showing  $s = 0, 0.25, 0.5, 0.75$  (solid black, blue, red, and green lines), where the three dashed black lines are indicating the equations  $f_t/\Delta\gamma = 10v/v_0, 4(v/v_0)^{1/2}, (v/v_0)^{1/4}$ , respectively. In other words, it seems the power law material with  $s = 0$  would only change results by a prefactor and hence, the agreement with experiments remains similar.

## 5 Conclusion

We have solved numerically the problem of rolling a rigid cylinder upon or under a rubber (viscoelastic) plane and compared the results with experimental findings by Barquins and his group with a simplified material model (standard linear solid). For sufficiently large Maugis–Tabor parameters  $\lambda$ , qualitative agreement was found for intermediate speeds in the friction force, although the contact area seems to increase less than in the experiments. With the help of the Persson–Brener theory of crack propagation, we have found quantitative prediction for the regime at low or intermediate velocities for large Maugis–Tabor parameter. In particular, the very low velocities show a linear dependence of the friction force on speed for both the bulk dissipation component and the adhesive hysteresis one. At low Maugis–Tabor parameters, the Persson–Brener model continues to be valid for the low to intermediate velocity range, although this may be only apparent since as we said the bulk hysteresis component is also linear with speed. Indeed, for low Maugis–Tabor parameters, the prefactor relating the cohesive strength to the cut-off stress of their theory depends on the other dimensionless parameters of the problem, making the theory less useful. It would seem that experimentally, only the intermediate regime was measured.

**Author Contributions** A. Papangelo conceived the presented idea, developed the theory and the computational model, and contributed to the final manuscript. R. Nazari obtained some results, discussed the results, and then contributed to the final manuscript. M. Ciavarella conceived the presented idea, developed the theory, and wrote the draft of the manuscript

**Funding** Open access funding provided by Politecnico di Bari within the CRUI-CARE Agreement. This work was partly supported by the Italian Ministry of University and Research under the Programme “Department of Excellence” Legge 232/2016 (Grant No. CUP - D93C23000100001). A.P. was supported by the European Union (ERC-2021-STG, “Towards Future Interfaces With Tuneable Adhesion By Dynamic Excitation” - SURFACE, Project ID: 101039198, CUP: D95F22000430006). Views and opinions expressed are however those of the authors only and do not necessarily reflect those of the European

Union or the European Research Council. Neither the European Union nor the granting authority can be held responsible for them. R.N. PhD scholarship was supported by the European Union (Next generation EU) within the Italian program PNRR.

**Data Availability** The dataset generated for this article is available on Zenodo at <https://zenodo.org/doi/10.5281/zenodo.10911323>.

## Declarations

**Conflict of interest** The authors declare that they have no known competing financial interests or personal relationships that could have appeared to influence the work reported in this paper.

**Open Access** This article is licensed under a Creative Commons Attribution 4.0 International License, which permits use, sharing, adaptation, distribution and reproduction in any medium or format, as long as you give appropriate credit to the original author(s) and the source, provide a link to the Creative Commons licence, and indicate if changes were made. The images or other third party material in this article are included in the article’s Creative Commons licence, unless indicated otherwise in a credit line to the material. If material is not included in the article’s Creative Commons licence and your intended use is not permitted by statutory regulation or exceeds the permitted use, you will need to obtain permission directly from the copyright holder. To view a copy of this licence, visit <http://creativecommons.org/licenses/by/4.0/>.

## References

1. Barquins, M.: Adherence and rolling kinetics of a rigid cylinder in contact with a natural rubber surface. *J. Adhes.* **26**(1), 1–12 (1988). <https://doi.org/10.1080/00218468808071271>
2. Maugis, D., Barquins, M.: Fracture mechanics and the adherence of viscoelastic bodies. *J. Phys. D Appl. Phys.* **11**(14), 1989–2023 (1978). <https://doi.org/10.1088/0022-3727/11/14/011>
3. Charmet, J.C., Barquins, M.: Adhesive contact and rolling of a rigid cylinder under the pull of gravity on the underside of a smooth-surfaced sheet of rubber. *Int. J. Adhes. Adhes.* **16**(4), 249–254 (1996)
4. Persson, B.N.J.: Rolling friction for hard cylinder and sphere on viscoelastic solid. *Eur. Phys. J. E* **33**, 327–333 (2010)
5. Schapery, R.A.: A theory of crack initiation and growth in viscoelastic media. *Int. J. Fract.* **11**(Part I), 141–59 (1975)
6. Persson, B.N.J., Brener, E.A.: Crack propagation in viscoelastic solids. *Phys. Rev. E* **71**(3), 036123 (2005)
7. Tabor, D.: Surface forces and surface interactions. *J. Colloid Interface Sci.* **58**(1), 2–13 (1977)
8. Maugis, D.: Adhesion of spheres: the JKR-DMT transition using a Dugdale model. *J. Colloid Interface Sci.* **150**(1), 243–269 (1992)
9. Johnson, K.L., Greenwood, J.A.: A Maugis analysis of adhesive line contact. *J. Phys. D Appl. Phys.* **41**(15), 155315 (2008)
10. Wu, J.J.: Adhesive contact between a cylinder and a half-space. *J. Phys. D Appl. Phys.* **42**(15), 155302 (2009)
11. Papangelo, A., Ciavarella, M.: Detachment of a rigid flat punch from a viscoelastic material. *Tribol. Lett.* **71**(2), 48 (2023)
12. Violano, G., Afferrante, L.: Size effects in adhesive contacts of viscoelastic media. *Eur. J. Mech. A Solids* **96**, 104665 (2022)
13. Papangelo, A., Ciavarella, M.: A numerical study on roughness-induced adhesion enhancement in a sphere with an

- axisymmetric sinusoidal waviness using Lennard-Jones interaction law. *Lubricants* **8**(9), 90 (2020)
14. Papangelo, A., Ciavarella, M.: Detachment of a rigid flat punch from a viscoelastic material. *Tribol. Lett.* **71**(2), 48 (2023)
  15. Afferrante, L., Carbone, G.: The ultratough peeling of elastic tapes from viscoelastic substrates. *J. Mech. Phys. Solids* **96**, 223–234 (2016)
  16. Schapery, R.A.: A theory of viscoelastic crack growth: revisited. *Int. J. Fract.* **233**, 1–16 (2022). <https://doi.org/10.1007/s10704-021-00605-z>
  17. Ciavarella, M., Cricri, G., McMeeking, R.: A comparison of crack propagation theories in viscoelastic materials. *Theoret. Appl. Fract. Mech.* **116**, 103113 (2021)
  18. Hui, C.Y., Zhu, B., Long, R.: Steady state crack growth in viscoelastic solids: a comparative study. *J. Mech. Phys. Solids* **159**, 104748 (2022)
  19. Persson, B.N.J.: Crack propagation in finite-sized viscoelastic solids with application to adhesion. *Europhys. Lett.* **119**(1), 18002 (2017)
  20. Persson, B.N.J.: On opening crack propagation in viscoelastic solids. *Tribol. Lett.* **69**(3), 115 (2021)
  21. Carbone, Giuseppe, Mandriota, Cosimo, Menga, Nicola: Theory of viscoelastic adhesion and friction. *Extrem. Mech. Lett.* **56**, 101877 (2022)
  22. Tiwari, A., Miyashita, N., Persson, B. N. J.: Rolling friction of elastomers: role of strain softening. *SoftMatter*. **15**(45), 9233–9243 (2019)

**Publisher's Note** Springer Nature remains neutral with regard to jurisdictional claims in published maps and institutional affiliations.